4-23-2019

Fibronectin-conjugated thermoresponsive nanobridges generate three dimensional human pluripotent stem cell cultures for differentiation towards the neural lineages.

Linda Harkness

Xiaoli Chen

Zhongfan Jia

Anthony M Davies

Michael Monteiro

See next page for additional authors

Authors
Linda Harkness, Xiaoli Chen, Zhongfan Jia, Anthony M Davies, Michael Monteiro, Peter Gray, and Martin Pera

Stem Cell Research 38 (2019) 101441

Contents lists available at ScienceDirect

Stem Cell Research

journal homepage: www.elsevier.com/locate/scr

Fibronectin-conjugated thermoresponsive nanobridges generate three dimensional human pluripotent stem cell cultures for differentiation towards the neural lineages

Linda Harkness[a,*], Xiaoli Chen[a], Zhongfan Jia[a], Anthony M. Davies[b], Michael Monteiro[a], Peter Gray[a], Martin Pera[c,d,e]

[a] Australian Institute for Bioengineering and Nanotechnology (AIBN), The University of Queensland, Brisbane, QLD 4072, Australia
[b] Translational Cell Imaging Queensland, Institute of Health and Biomedical Innovation, Queensland University of Technology, Brisbane, QLD 4102, Australia
[c] The Florey Institute of Neuroscience and Mental Health and the Walter and Eliza Hall Institute of Medical Research, Parkville, Victoria 3052, Australia
[d] The Jackson Laboratory, Bar Harbor, ME 04609, United States
[e] The University of Melbourne, Melbourne, Victoria 3010, Australia

ARTICLE INFO

Keywords:
hESC
3D cell culture
Neural progenitors
Thermoresponsive polymer

ABSTRACT

Production of 3-dimensional neural progenitor cultures from human pluripotent stem cells offers the potential to generate large numbers of cells. We utilised our nanobridge system to generate 3D hPSC aggregates for differentiation towards the neural lineage, and investigate the ability to passage aggregates while maintaining cells at a stem/progenitor stage. Over 38 days, aggregate cultures exhibited upregulation and maintenance of neural-associated markers and demonstrated up to 10 fold increase in cell number. Aggregates undergoing neural induction in the presence or absence of nanobridges demonstrated no differences in marker expression, proliferation or viability. However, aggregates formed without nanobridges were statistically significantly fewer and smaller by passage 3. Organoids, cultured from aggregates, and treated with retinoic acid or rock inhibitor demonstrated terminal differentiation as assessed by immunohistochemistry. These data demonstrate that nanobridge 3D hPSC can differentiate to neural stem/progenitor cells, and be maintained at this stage through serial passaging and expansion.

1. Introduction

Neurodegenerative diseases (e.g. neurological disorders and dementias) result in progressive loss of structure and neurological function, including the death of neurons. Dementia is expected to pose a significant health and socio-economic burden, estimated to affect 131.5 million people in 2050 and costing a trillion US dollars in 2018 alone (Martin et al., 2015). Current treatment of degenerative brain diseases are based on imprecise symptomatic treatment (Chen and Pan, 2014). This limitation has driven an intensive search for new therapeutic interventions, including the use of human pluripotent stem cells (hPSC). These cells can be used as a platform for drug development or as a source for cellular therapies, with the potential to transform approaches to injury treatment, disease management and drug discovery. Expansion of hPSC to the cell numbers required for these applications remains a critical challenge. Of equal importance is the differentiation of hPSC to progenitor cells of particular lineages and their subsequent expansion to large cell numbers required for clinical and pharmacological use. While two dimensional (2D) monolayer cell cultures continue to be utilised in the majority of stem cell expansion systems, three dimensional (3D) cultures of hPSC have been demonstrated to far outperform 2D cultures for scale-up (Chen et al., 2012; Chen et al., 2014). Culturing cells in 3D provides a more physiologically relevant environmental niche and can offer a more realistic model of the developmental processes in differentiation and the cell-cell interactions involved (Akkerman and Defize, 2017).

Differentiation of hESC towards neuronal lineages has been extensively studied, with current methods increasingly using small molecule inhibitors to tightly regulate initial stages of differentiation and to aid in supplying a more precise temporal control for downregulation of pluripotency markers (Chambers et al., 2012; Wattanapanitch et al., 2014). Many monolayer differentiation and expansion methods for neural progenitors include labour intensive and time-consuming manual dissection. This limits the available cell numbers, and

* Corresponding author.
E-mail address: l.harkness@uq.edu.au (L. Harkness).

https://doi.org/10.1016/j.scr.2019.101441
Received 27 January 2019; Received in revised form 31 March 2019; Accepted 15 April 2019
Available online 23 April 2019

additionally, as 2D cultures cannot emulate the natural 3D environment they may result in misleading outcomes when utilizing results as a predictive response for in vivo applications (Edmondson et al., 2014). Advances in CNS organoid culture have allowed the observation of specific morphogenetic events in brain development, and have provided insights into cell interactions that are beneficial for modelling and histotypic differentiation (Jo et al., 2016; Kelava and Lancaster, 2016; Lancaster et al., 2013; Werner et al., 2016). Recent data has demonstrated that implantation of brain organoids in mouse brain demonstrate both functionality and vascularisation (Mansour et al., 2018). However, many organoid culture systems lack reproducibility, and present challenges when the structures must be dissociated for single cell analysis (Huch et al., 2017).

The generation of neural stem or progenitor cells (NPC) and their subsequent differentiation to terminal cell types using 3D cultures and scaffolds have been reported. These include methods utilizing hydrogels (Li et al., 2012; Adil et al., 2017; Rodrigues et al., 2017), alginate (Bozza et al., 2014) and fibrin matrix (Sadri et al., 2014); or passive aggregation in the absence of supporting materials (Chandrasekaran et al., 2017). Li et al. demonstrated that the larger pore size methacrylamide chitosan hydrogel photocrosslinked to D-mannitol could support differentiation of NPC to neurons, oligodendrocytes and astrocytes; however, these large pore sizes led to decreased cell numbers (Li et al., 2012). Adil et al. and Rodrigues et al. both utilised commercial hydrogels (Mebiol gels, Adil et al., 2017; PNIPAAm-PEG, Rodrigues et al., 2017) to establish 3D hESC aggregates, subsequently differentiating cells towards dopaminergic neurons and oligodendrocyte precursors respectively. Encapsulation of mouse ESC in alginate beads using hyaluronic acid (HA) or fibronectin (FN) enhanced the differentiation ability of the cells (Bozza et al., 2014). HA combined with alginate and alginate alone increased neuronal differentiation of the cells as compared to FN treated alginate (Bozza et al., 2014). Sadri et al. demonstrated a reduction of apoptosis in 3D as opposed to 2D cultures (Sadri et al., 2014). When directly comparing 2D versus 3D cultures, Chandrasekaran et al. demonstrated increased neuron numbers, process length and glial progenitor formation in 3D cultures of differentiating hPSC (Chandrasekaran et al., 2017). Although this body of work demonstrated the advantages of 3D systems to differentiate mouse and human PSC towards neuronal cells, aggregate size was not controlled, a factor that can result in necrotic cores becoming established in nutrient deficient areas. Importantly the above studies were designed to investigate terminal differentiation, did not investigate if neural progenitor cells could be maintained during serial passaging, and routine passaging was performed using enzymatic or non-enzymatic methods.

The work presented here addresses the critical need to develop a 3D expansion method that facilitates aggregation and offers the capacity to control aggregate size by passaging during differentiation. Using our method, aggregates can then be easily grown in a cyclic manner for rapid expansion to obtain large cell yields, while maintaining the cells in the state of choice. This method overcomes reported issues in low efficiency in formation of aggregates and control over aggregate size (Chandrasekaran et al., 2017).

Here, we demonstrate a 3D cell culture method that allows hPSC to be differentiated to, and expanded as, NPC. Previous publications have demonstrated the presence of necrotic cores in cancer spheroids of ≈ 500 μm (Daster et al., 2017; Hirschhaeuser et al., 2010), thus, we investigated if controlling aggregate size prevented the formation of a necrotic core and, additionally, if the aggregates could differentiate towards a terminal neuronal phenotype. The 3D culture system consisted of a thermoresponsive nanobridge system (NB) allowing a temperature shift to be utilised in conjunction with a low mechanical shear to dissociate the aggregates to smaller clumps (i.e. without the addition of enzymatic treatment) (Chen et al., 2017; Chen et al., 2014). Neural differentiation was initiated when aggregates reached an average diameter between 200 and 300 μm. Passaging was performed throughout the culture period maintaining an average diameter of between 300 and 450 μm. We investigated if using this method could maintain the aggregates at the neural stem/progenitor stage and tested the efficacy of the differentiation against conventional monolayer cultures of hPSC undergoing neural induction. Our 3D culturing method provides a more robust and less labour intensive approach for generating and maintaining differentiated hPSC as neural stem/progenitor cells, and has the potential for large-scale production.

2. Materials and methods

2.1. Cell culture and aggregate formation

hESC (WA09 (WiCell Research Institute Inc), ESI-hES3 (Embryonic Stem Cell International Pte Ltd., Singapore), and MEL1 (University of Queensland)) were routinely cultured as adherent cells in mTeSR1 media (STEMCELL Technologies) on Matrigel™ coated wells (MG™; Corning). To generate 3D aggregates for culture in a 96 well platform, 2D cells were washed with phosphate buffered saline without Ca^{2+} and Mg^{2+} (PBS2-) and dissociated to single cells using TrypLE (Thermo Fisher Scientific). Cell counts were performed and 70,000 cells/ml were mixed with the NB components (50 μg/ml PNIPAM-b-rFN, 50 ng/ml of the pWorms) as previously described (Chen et al., 2014). Detailed protocols to determine the polymer concentrations can be found in Chen et al. (Chen et al., 2017). The combination of both polymer components is referred to as NB. 50 μl aliquots of cells at a concentration of 70,000 cells/ml, with or without NB, were aliquoted into 60 wells of a 96 well U shaped low attachment culture dish (Corning) and centrifuged at 37 °C for 5 mins at 480 G. Plates were incubated at 5% CO_2, 37 °C overnight and examined the following day for aggregate formation.

For 6 well cultures, hESC were passaged using Gentle Cell Dissociation reagent (STEMCELL Technologies) to produce small clumps of cells. Cells were mixed with the above-mentioned NB concentrations, and incubated overnight at 5% CO_2, 37 °C in 6 well low cluster plates (Corning). Cell counts were performed on the day differentiation was initiated. A maximum of 2× sub confluent 2D wells from a 6 well plate were used to generate 1 well of a 6 well 3D culture.

2.2. Neural induction

Neural induction for both 96 and 6 well cultures was started (day 0) when the average aggregate width was between 200 and 300 μm. Differentiation was based on a modification of the method published by Chambers et al. (Chambers et al., 2009) where 100 nM LDN 193189 (Stemgent Inc.) replaced Noggin. Briefly, aggregates were cultured in 5 μM SB431542 (Miltenyi Biotech) and 100 nM LDN 193189 (Stemgent Inc.) in mTeSR1 media for 5 days. At d5 the medium was changed to neural basal media (with 1× B27, 1× N2, 1× ITS-A, 1× Glutamax (NBM; all Invitrogen)) and supplemented with 20 ng/ml EGF (PeproTech) and 20 ng/ml FGF2 (Invitrogen) for the next 5 days of culture. This protocol was utilised as the base method for all routine cultures performed in NBM, FGF2 and EGF were withdrawn from d10 onwards. Passaging was performed at d10 and, thereafter, on a weekly basis. Six well cultures were grown under static conditions. To decrease the possibility of aggregates clumping under static conditions and to maintain the maximum average aggregate width at passage of ≈ 450 μm, cultures were passaged at d5 and d10 during induction, and thereafter on a weekly basis.

To examine the effect of neural growth factors FGF2 and EGF on the 3D culture system single aggregates, cultured in a 96 well format in NBM, were supplemented with EGF alone, FGF2 alone, EGF/FGF2 added weekly, daily or a sustainable form of FGF2 (with EGF) added twice weekly (Speed BioSystems, Maryland, USA).

2.3. Terminal differentiation

To establish if 3D NB aggregates could yield terminally differentiated cells, WA09 96 well cultures underwent dual SMAD inhibition and neural induction with EGF and FGF2 before supplementation with either Rock inhibitor Y27632 (25 μM, RI, Miltenyi Biotech) or retinoic acid (50 μM, RA, Sigma-Aldrich) for a maximum of 12 weeks of culture. Samples were taken at weeks 4 (d38), 8 (d66) and 12 (d94) for RT-PCR and at week 8 and 12 aggregates were manually dissociated and allowed to outgrow for 5 days in NBM alone before staining.

2.4. Proliferation, viability and aggregate diameter

To examine proliferation and aggregate growth, cell counts were performed at d5, d10 and prior to passaging on a weekly basis (p1d7 etc). Proliferation was calculated using seeding density of aggregates on the day of induction (d0) as baseline and for generating fold expansion for each data point (over d0 data). Viability was assessed using Trypan Blue. To calculate diameter, aggregates were imaged on a Nikon Eclipse Ti-U inverted microscope using automated acquisition for imaging and to stitch images together (NIS-Elements, Nikon). Individual images were outlined in Photoshop using the elliptical marquee or lasso tools and aggregate width was calculated using the Photoshop analysis tool. For the purposes of this manuscript 'diameter' is used as the measure. Measurement scale was set using the NIS Element generated scale bar and the diameter data generated in μm. Minimally, 3 independent experiments were performed with 60 aggregates analysed per experiment at each time point.

2.5. Gene expression

Samples for RT-PCR were taken at d0, d5, d10, and thereafter on a weekly basis (passage 1 (p1), p2, p3, p4). As an indicator of differentiation efficiency under 3D conditions WA09 were cultured as 2D using the above base method (without passaging) and samples taken for RT-PCR at the same time intervals. A minimum of 3 experiments were performed for each cell line as 96 or 6 well or 2D cultures.

RNA was extracted from aggregates using an RNeasy purification mini kit (Qiagen) including treatment using an RNase-free DNase set (Qiagen) according to manufacturer's instructions. cDNA was generated using a RevertAid First Strand cDNA synthesis kit (Thermo Fisher Scientific) according to manufacturer's instruction. RT-PCR was performed on 10 μg of cDNA for each reaction with 2× Fast SYBR green master mix (Applied Biosystems) using a 7500 fast real-time PCR machine (Applied Biosystems). Cycle threshold (CT) values for each primer set were normalised to a geometric mean of four housekeeping genes (βActin, TBP, B2M, HPRT1) and analysis performed using the comparative ΔΔCT method. Data is plotted as expression relative to the geometric mean of all housekeeping genes. Primer sets were purchased from either GeneWorks, (Thebarton, South Australia) or Integrated DNA Technologies (Singapore) and included *POU5F1* (Octamer-binding transcription factor 4), *NANOG*, *DNMTB3* (DNA methyltransferase 3 beta), *PAX6* (paired box protein 6), *SOX1* (SRY-Box 1), *NCAM* (neural cell adhesion molecule), *HOXA3* (homeobox protein HOX-A3), *MAP2* (microtubule-associated protein 2) and *DCX* (Doublecortin). In addition, aggregates cultured in media supplemented with either RI or RA were examined for expression of *GFAP* (Glial fibrillary acidic protein), *S100B* (S100 calcium-binding protein B), *FOXD3* (Forkhead box protein D3), *NEUROG1* (Neurogenin-1), *HOXA3* and *EN1* (Engrailed-1).

2.6. Immunostaining

To establish if a necrotic core formed during culture, intact aggregates, at each passage, were stained for 1–2 h at 37 °C, 5% CO_2 in 10 μg/ml Hoechst 33342 or CyQUANT (diluted 1:10 in culture media instead of 1:2, otherwise prepared according to manufacturer's instructions) and 10 μM DRAQ7 before imaging using the IN Cell Analyzer 2200 (GE Healthcare). Eleven to 15 slices, with a 5 μm distance between slices, were imaged and deconvoluted. Images were loaded in ImageJ, stacked and processed using the Z project to create one image from the slices, in addition, a surface plot of live and dead cells was created using ImageJ-Fiji (Schneider et al., 2012).

To ascertain if downregulation of POU5F1 protein could be observed in intact aggregates and if differentiation occurred throughout the aggregate or at specific locations (central or peripheral) daily samples were taken over the initial 5 day period (d0-d4 of SMAD inhibition). Samples were washed in PBS2-, fixed and washed 3× in PBS2- (30 mins for fixation and all washes). To enhance the clarity of the 3D aggregate, ScaleA2 (Hama et al., 2011), a solution which allows optical clearing, was utilised prior to staining. Post fixation, aggregates were incubated overnight in a 20% sucrose solution and then transferred to Scale A2 for two further days. Both incubations were performed at room temperature. To provide comparable data for 3D measurement of protein expression, aggregates between d0 and d4 were dissociated by manual pipetting, plated onto pre-coated MG™ Nunc F (flat) 96 well plates (Thermo-Fisher Scientific), and incubated overnight at 37 °C, 5% CO_2. The following day wells were washed in PBS2-, fixed in 10% formalin, and washed a further three times in PBS2- (minimum of 5 mins/wash).

3D aggregates were incubated in blocking buffer (PBS2-, 0.1% TritonX-100, 4% normal goat serum) at room temperature (RT) for 4 h before addition of primary antibody (mouse) POU5F1, recognising the A isoform related to pluripotency (Wang and Dai, 2010) (2 μg/ml; Santa Cruz (SC); C-10; sc-5279). Aggregates with antibody were incubated overnight, in staining buffer (PBS2-, 0.1% TritonX-100, 1% bovine serum albumin) at 4 °C. The aggregates were washed 3× in PBS2- before incubation with a goat anti-mouse 488 Alexa Fluor secondary (2 μg/ml, Thermo Fisher Scientific) for 4 h at RT; again washed 3× in PBS2- and placed in 10 μg/ml Hoechst 33342. Aggregates were then transferred, in Hoechst 33342, to a 384 well plate at 1 aggregate/well and 5 aggregates/time-point, for 4 biological replicates (n = 4).

For dissociated and replated aggregates d0–4 of 96 well cultures (WA09 only), d0, d5, d10, p1, p2, p3 and p4 from 6 well cultures (WA09, ESI-hES3, MEL1)) and terminal differentiated aggregates (WA09 only) a similar staining protocol to that above was utilised, however there was no pre-treatment with sucrose and ScaleA2. Primary antibodies (mouse POU5F1 (SC), mouse PAX6 (3.5 μg/ml, Developmental Studies Hybridoma Bank), rabbit SOX1 (1:400 dilution, #4194, Cell Signalling), mouse MAP2 (2.5 μg/ml, AP20, MAB3418, Millipore)) and mouse Tubulin, Beta III (1:400 dilution, EMD Millipore, clone TU-20) were incubated overnight at 4 °C. Incubation in blocking buffer and Alexa Fluor secondaries (goat anti-mouse or goat anti-rabbit) were carried out for 2 h at RT. DRAQ5 (10 μM, AbCam) or Hoechst 33342 (10 μg/ml) were used as nuclear stains for 30 mins at RT and all washes were performed for 5 mins in PBS2-.

Organoids cultured for terminal differentiation were fixed, histologically processed, and embedded in paraffin wax before sectioning at 5 μm. Sections were stained, using an antigen retrieval method, with PAX6 (rabbit, 1:50 dilution, AbCam), MAP2 (rabbit, 1:3000 dilution, AbCam), Tubulin, Beta III (mouse, 1:100 dilution, Santa Cruz Biotechnology), Nestin (rabbit, 1:400 dilution, Santa Cruz Biotechnology), GFAP (mouse,1:50 dilution, Cell Signalling) and anti-Oligodendrocyte protein (rabbit ab53041,1:500 dilution, AbCam). Alexa Fluor secondaries (goat anti-mouse or goat anti-rabbit) were utilised at 1:500 and sections were counterstained with Hoechst. Fluorescent images of stained organoids were scanned using a Nikon Eclipse Ni microscope at 20× magnification.

2.7. Imaging and analysis of fluorescent staining

Imaging was performed on an InCellAnalyzer 2200 and analysis carried out using IN Cell Investigator software (both GE Healthcare). 3D

and 2D aggregate imaging was performed at 20× magnification. For 3D antibody stained aggregates an average number of 11–15/aggregate z-slices were acquired at a distance of 5 μm between slices; 3D deconvolution was performed automatically during and following acquisition of images. Replated aggregate imaging was performed across 9 fields centrally placed with fixed spacing per field. All images were analysed using the Multi Target Analysis module and a threshold filter selected for each antibody to provide data for the number of positive and negative cells. Unstained or secondary only stained wells served as a baseline for detecting positively stained cells.

2.8. Thermoresponsive nanobridges

We have previously reported the generation of 3D aggregates from 2D hESC cultures utilizing a thermoresponsive nanobridge system consisting of (i) a block copolymer of a thermoresponsive poly(N-isopropylacrylamide) (PNIPAM) polymer conjugated to a fibronectin (FN) fragment (PNIPAM-b-FN) and (ii) thermoresponsive polymer nanoworms (pWorms) with a PNIPAM corona (Chen et al., 2017; Chen et al., 2014). A reduction of temperature to 32 °C, which is below the lower critical solution temperature (LCST) of the PNIPAM chains, causes the PNIPAM to become water-soluble, allowing cell-cell binding to weaken. Cell aggregates can then be broken into small clumps by exerting a low shear force. This allows passage in a suspension culture system without recourse to enzymatic or non-enzymatic dissociation solutions.

2.9. Statistical analysis

Statistical tests were performed on staining data following IN Cell Investigator analysis with cell counts, aggregate width, viability and transcript expression parameters used to establish levels of significance. Data sets were loaded in GraphPad Prism and multiple comparisons performed using a one-way ANOVA with a Tukey test post ANOVA, and multiple *t*-tests using the Holm-Šídák method to correct for multiple comparisons. Reported levels of significance were * $p < 0.05$, ** $p < 0.01$, *** $p < 0.005$ and **** $p < 0.001$.

3. Results

Experiments were established to investigate (i) if consistently sized aggregates could be generated at a high formation rate using the NB; (ii) if the NB components influenced the differentiation of hESC aggregates; (iii) if neural induction in 3D-hESC NB aggregates cultured on either a 96 or 6 well platform demonstrated equivalent differentiation capacity to 2D monolayer cultures; (iv) if culturing cells in 3D induced the formation of a necrotic core; (v) if the 3D-hESC NB neural induced aggregates could become terminally differentiated. A diagram depicting the method for formation, culture and disaggregation can be found in Fig. 1A.

3.1. Comparison of 96 well cultures with and without nanobridges in hESC undergoing neural induction

Cultures in 96 well plates were established to determine if 3D aggregates could be differentiated to neural progenitors and if the NB components effected neuronal differentiation.Cultures of WA09 were harvested and resuspended as a single cellsuspension, mixed with or without the NB components, aliquoted in a 96 well plate, centrifuged and incubated. The aggregate formation rate was high with > 98% formation in aggregates with and without the NB components. Aggregates were cultured in the absence or presence of NB in mTeSR1 until anaverage aggregate diameter of ≈ 300 ± 5.9 μm was achieved. Neural induction was then initiated (d0) and aggregate diameter monitored and analysed using a one-way ANOVA. No statistically significant differences, with or without NB components respectively, were determined in percentage cell viability (90.6 ± 4.3 vs 88 ± 4.4; mean ± SD) or proliferation (7.6 ± 1.31 vs 7.6 ± 0.90; mean ± SD) (Supplementary Fig. S1Ai). Aggregate diameter was statistically significantly smaller in cells cultured in the absence of NB components at d5 and p3 ($p < 0.001$); no significant differences were found at other time points (Supplementary Fig. S1Ai). Supplementary Fig. S1Aii shows images of NB generated aggregates at days 0, 5, 10, passages 1–3.

ANOVA analysis of proliferation data over time, with or without NB, demonstrated significantly increased proliferation rate for both conditions between d0 or d5 and d10, p1, p2 and p3 ($p < 0.005$). Analysis between d10 and further time points demonstrated that the proliferation rate did not significantly increase (Supplementary Fig S1Ai). Aggregate diameter, analysed between sample time points, statistically significantly increased between d0 and d5, and d5 and d10 ($p < 0.001$), and statistically significantly decreased between p1 and p2, and p2 and p3 ($p < 0.001$) irrespective of addition of NB. No significant difference in aggregate diameter could be found between d10 and p1. A summary of the statistics are in Supplementary Table S1.

Experiments were terminated at passage 3 day 7 (p3d7) following decrease of proliferation and concurrent decreases in aggregate diameter irrespective of the addition of NB. No differences were found between cultures with or without NB when gene expression was examined (*POU5F1*, *NANOG*, *DNMT3B*, *PAX6*, *SOX1*, and *NCAM*) (Supplementary Fig. S2A). Staining at p3 demonstrated a few PAX6 positive cells in aggregates formed without NB and limited numbers of MAP2 positive neurites in aggregates created with and without NB suggesting that majority of cells had exited the stem cell stages (Supplementary Fig. S2B).

It became increasingly difficult to manually disaggregate cells cultured without NB components as passage number increased suggesting that, as previously reported (Chen et al., 2017), the polymer played a role in the ability to dissociate aggregates. The percentage of aggregates that reformed at p3d1 was significantly less in cultures without NB (p3d1 with NB: 88.3% ± 12.6 cf. without NB: 54.6% ± 20.2%; $p < 0.05$) suggesting a need for the NB in re-aggregation. Additionally, the diameter of aggregates reformed without NB were significantly smaller at p3d7 ($p < 0.001$) than those reformed with NB. Significant differences were not found at any other time point for aggregate formation. Representative images detailing differences between NB and cultures without polymer at p3d7 can be found in Supplementary Fig. S1B.

3.2. Proliferation, aggregate diameter and viability in static 6 well cultures of hESC undergoing neuronal differentiation

To ascertain if the 96 well platform was scalable WA09, ESI-HES3 and MEL1 were established as multi aggregate cultures in a static 6 well format. Following passaging with Gentle Cell Dissociation reagent small clumps of hESC were mixed with NB components and cultured in low cluster 6 well plates. From data acquired in the 96 well plate format, we determined that (1) aggregates differentiated into neural stem/progenitor cells; (2) there were limited differences in proliferation, transcript expression or aggregate diameter between cultures with and without NB components (Supplementary Figs. S1 and S2). This established thatthe NB components had no influence on the differentiation capacity of 3D cultured hESC. Thus,scale up to 6 well cultures was performed for NB cultures alone.

WA09 cultures using thestatic 6 well culture platform (Fig. 1B, n = 4) continued proliferation until the termination of the experiment (p4d7) as compared to the 96 well format. Proliferation (7.5 ± 2.2 fold expansion at p4d7; mean ± SD) increased across the experimental periodwith statistical significance demonstrated between d0 and p1 ($p < 0.05$), d0 and p2 ($p < 0.005$); d0 and p3 and d0 and p4 ($p < 0.001$). No significant difference was determined in percentage cell viability across the culture period (93.7 ± 1.6; mean ± SD). Aggregate diameter was regained after each passage and only decreased significantly at the end of the culture period (between d5 and p3d7

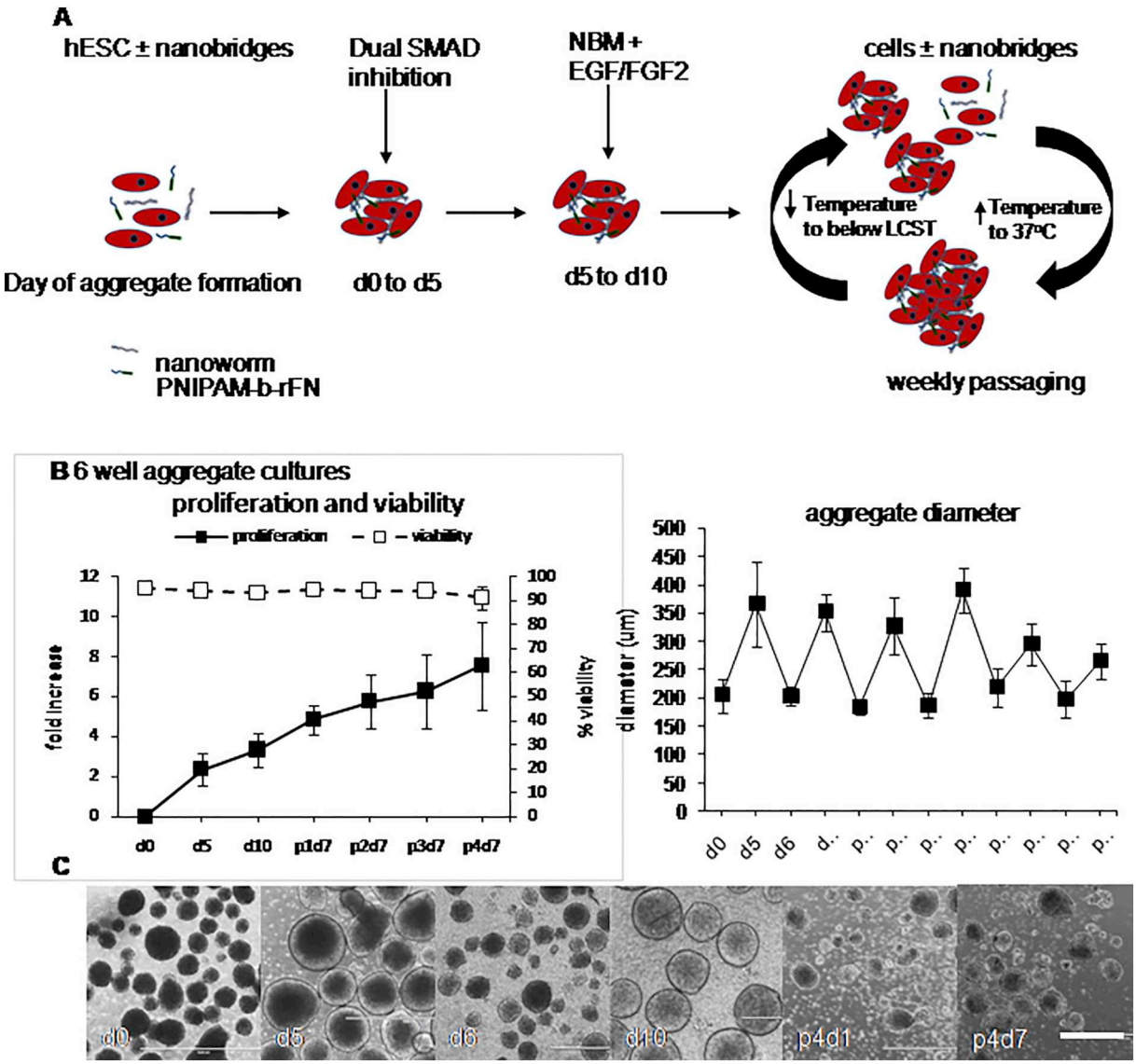

Fig. 1. 3D culture of hESC undergoing neuronal induction. A. Diagram depicting the basic method for creation and maintenance of hESC with or without nanobridges to aggregate and dissociate the hESC. B.6 well culture platform: WA09 were dissociated to small clumps, mixed with the nanobridges, and cultured to form aggregates overnight; passaging was performed at d5, d10 then weekly (i) graphs depicting cell viability, fold proliferation and aggregate diameter (μm); (ii) micrographs depicting changes in aggregate width during culture. Scale bar = 500 μm; LCST = lower critical solution temperature; n = 3 independent experiments, mean ± standard deviation (SD).

$p < 0.005$; and d5 and p4d7 $p < 0.001$). Images from aggregates undergoing initial induction and following final disaggregation (p4d1) and final growth (p4d7) can be seen in Fig. 1B.

Two additional hESC lines (ESI-hES3 and MEL1; Supplementary Fig. S3) were differentiated as static 6 well cultures. Both cell lines showed similar patterns to the WA09 in viability, proliferation and recovery of aggregate diameter following passaging. Statistics for proliferation and diameter for the single and multi-aggregate cultures are reported in Supplementary Table S1.

3.3. Gene expression analysis of monolayer and 3D (96 well and 6 well) neuronal cultures

Gene expression analysis (Fig. 2 and Supplementary Figs. S2, S4 and S5) demonstrated significant downregulation ($p < 0.01$; d0 vs d10) of pluripotency markers *POU5F1*, *NANOG*, and *DNMT3B* in all three cell lines and across different culture conditions (2D adherent monolayer, 3D in 96 well and 3D static 6 well). No significant differences could be detected between NB and no polymer cultures in transcript levels of *PAX6*, *SOX1* or *NCAM* (Supplementary Fig. S2). In WA09, 2D monolayer cultures demonstrated slower downregulation at d5 of both *NANOG* and *DNMT3B* as compared to both 96 and 6 well 3D cultures. Increased transcript levels for genes associated with early neural differentiation, (*PAX6*, *SOX1 and NCAM*) were observed in cells cultured as 3D aggregates as compared to 2D monolayer cultures however these were not significant for *SOX1* (Fig. 2, Supplementary Table S3). While ESI-hES3 and WA09 demonstrated similar patterns of gene expression for all genes analysed (*PAX6*, *SOX1*, *NCAM*, *HOXA3*, *DCX*, *MAP2*), MEL1 demonstrated a different profile for *PAX6* where significant downregulation was observed at p2 ($p < 0.005$), however protein expression of *PAX6* could still be observed at p4 (Supplementary Fig. S5). *DCX* has been reported to identify postmitotic neurons with inhibited proliferation and migratory potential (Filipovic et al., 2012). Rises in transcript levels of *DCX* in combination with *HOXA3* were observed in all 6 well static cultures towards the end of the culture period with a few cells demonstrating *MAP2* positive neurite outgrowth. *HOXA3* and

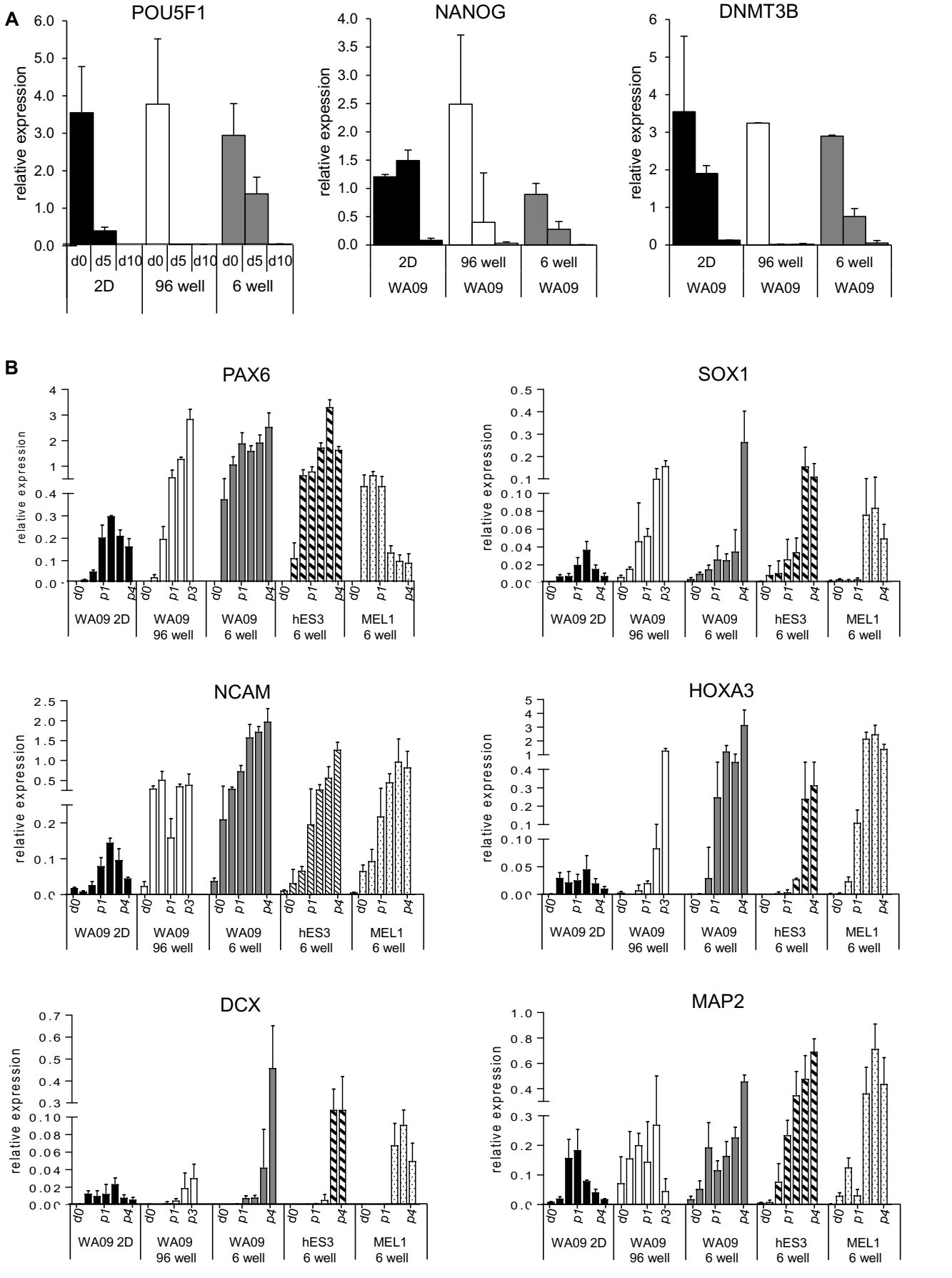

(caption on next page)

Fig. 2. Gene expression of monolayer and 3D hESC cultures undergoing neuronal differentiation. A. down regulation of pluripotency markers POU5F1, NANOG and DNMT3B in WA09. B. Regulation of neuronal markers PAX6, SOX1, NCAM, HOXA3, DCX and MAP2 in monolayer (2D) and 3D cultures over a total of 38 days of differentiation. Gene expression, relative to the geometric mean of the housekeeping gene panel, demonstrate that 3D cultures are more efficacious that 2D for neuronal differentiation. n = 3 independent experiments, mean ± SD.

MAP2 are associated with hindbrain development (Philippidou and Dasen, 2013) and stabilisation of microtubules (Dehmelt and Halpain, 2005) suggesting that, when combined with slowing proliferation and aggregate width, that a few cells were progressing towards, and past, the post-mitotic stage.

3.4. Staining and analysis of replated and intact 96 well cultured aggregates

High content imaging and analysis (HCA) allows rapid and automated image acquisition that can be used to detect changes in cellular morphology and investigate protein expression in individual cells. We utilised HCA to investigate the presence/absence of a necrotic core and to establish how efficiently the POU5F1 protein was down regulated within NB aggregates during early differentiation.

Imaging of live and dead cells in intact aggregates did not show a concentration of dead cells in the centre of the aggregate, rather DRAQ7 positive cells were evenly distributed throughout the aggregate suggesting that a necrotic core was not established. Comparison of live/dead cell counts from InCell analysis equated with manual cell counts (Supplementary Fig. S6C). To provide an overall impression of the location of the dead cells, images at p3 were loaded in ImageJ, stacked and processed using the Z project to create one image from all slices (Supplementary Fig. S6A) (Schneider et al., 2012). This demonstrated an even distribution of dead cells throughout the aggregate. In addition, a 3D surface plot of CyQUANT (black) and DRAQ7 (white) was created in ImageJ-Fiji through 50% of an aggregate to further verify the even distribution of dead cells within aggregates (Supplementary Fig. S6B).

Intact and replated (overnight) WA09 96 well aggregates were examined for POU5F1 protein expression and location between d0 and d4 of differentiation. Analysis was performed on multiple slices (11–15/aggregate) taken through intact aggregates (5 aggregates per condition, n = 4 independent experiments) and on images taken from 9 fields/well of replated 3D aggregates (minimum of 3 wells/experiment, n = 4 independent experiments). As demonstrated in Supplementary Fig. S7, similar patterns for down-regulation of POU5F1 were identified at each time-point between aggregates analysed intact and those examined following replating. Induction of differentiation, as measured by POU5F1 staining, occurred uniformly throughout the aggregates.

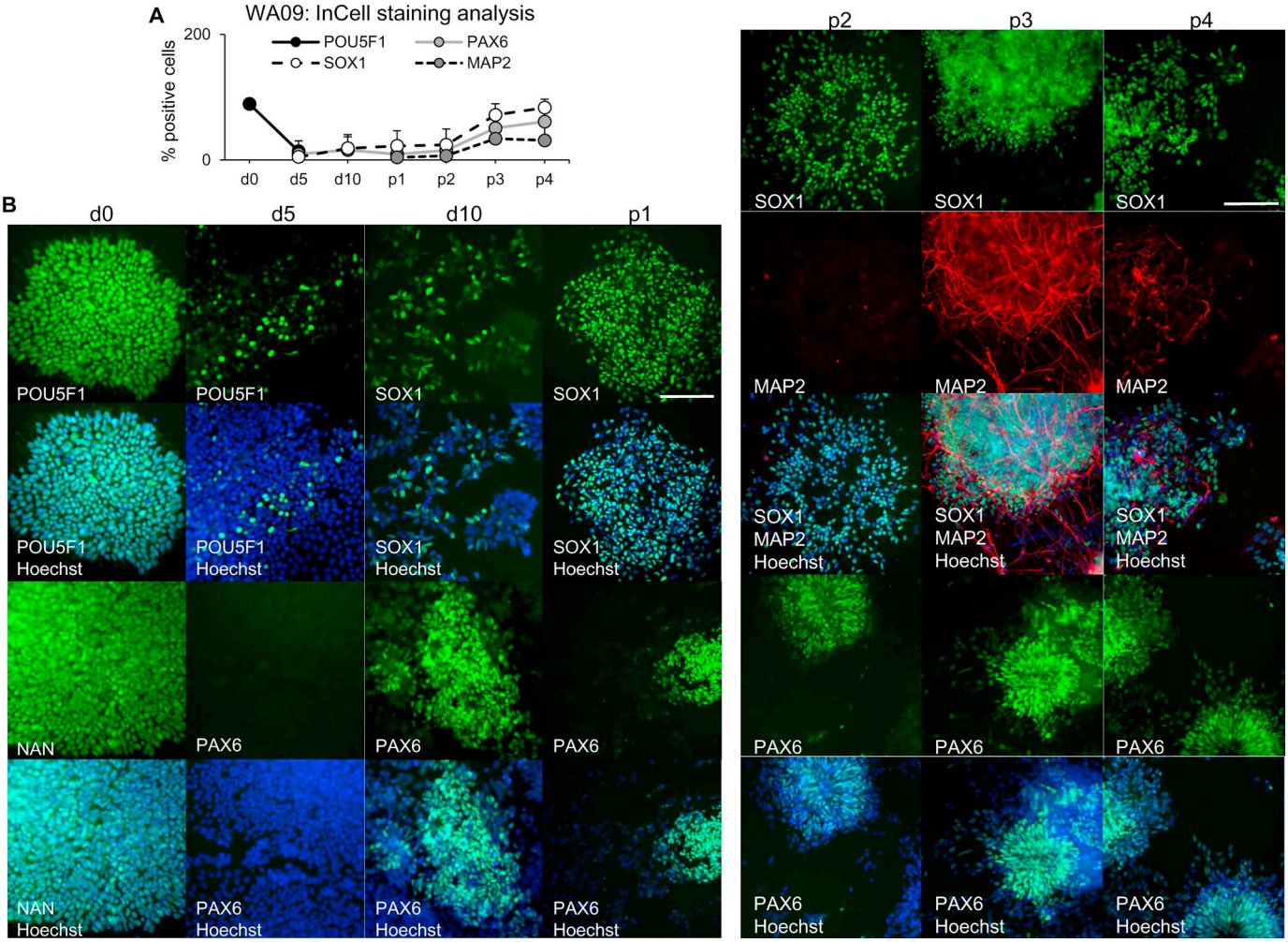

Fig. 3. Staining and analysis of replated WA09 3D aggregates for POU5F1, Nanog, PAX6, SOX1 and MAP2 at d0, d5, d10, p1, p2, p3 and p4 of neuronal differentiation cultured using the 6 well culture platform. A. Analysis of staining demonstrating the % of positive cells counted in high content screened images. B. Images demonstrate staining for each antibody (AB) and a merged image of AB with Hoechst for pluripotency markers at d0 and d4 and neural markers from d5 of differentiation. Scale bar = 100 µm. n = 4 independent experiments, data plotted as mean ± SD.

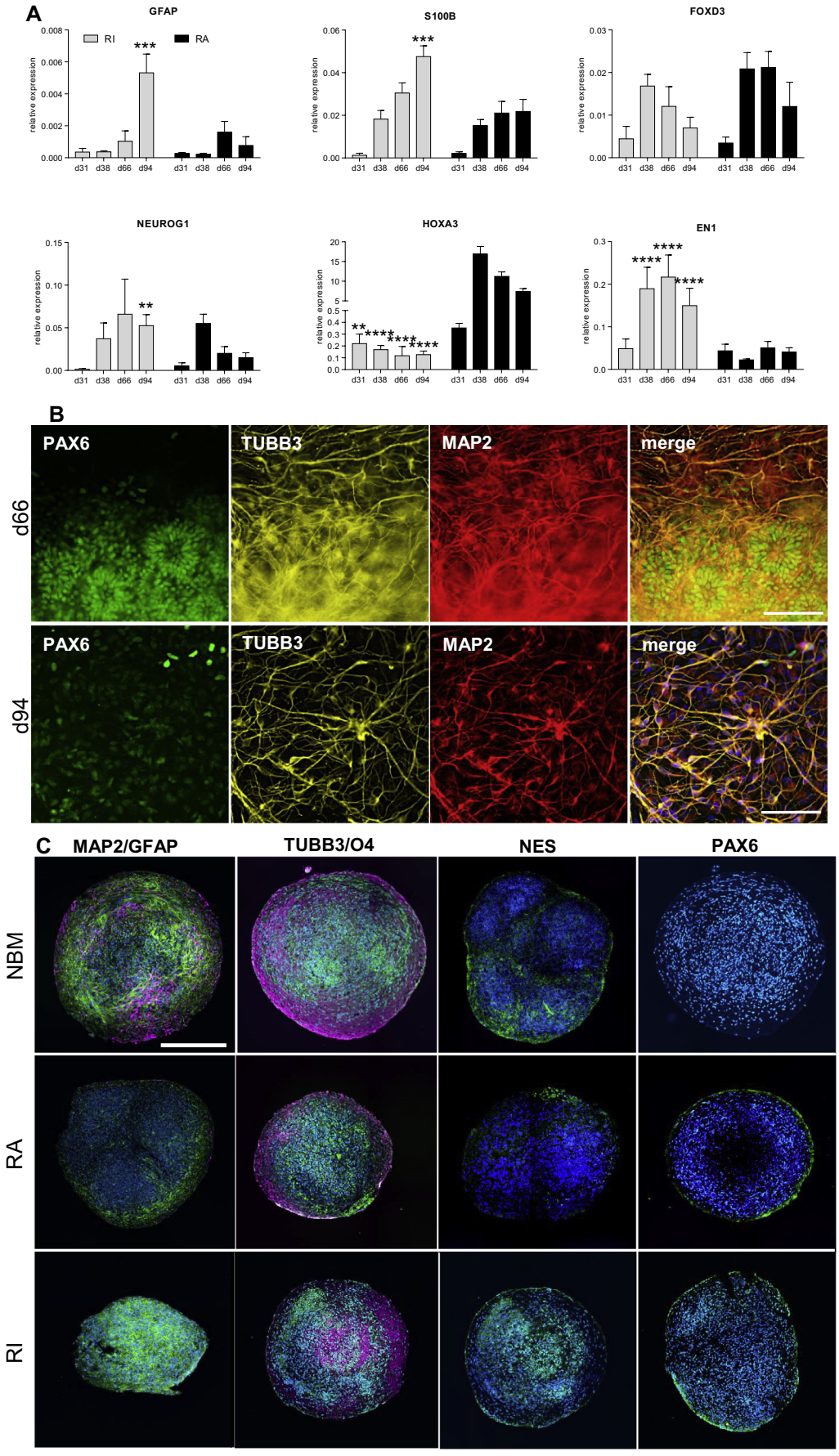

Fig. 4. Organoid differentiation of 3D nanobridge hESC cultures in NBM or supplemented with RI and RA. A. Relative gene expression of differentiation markers GFAP, S100B, FOXD3, NEUROG1, HOXA3 and EN1 at days 31, 38, 66 and 94 of differentiation. Upregulation of GFAP, S100B and NEUROG1 was observed in RI when compared to RA treated cultures at d94; EN1 demonstrated upregulation in RI treated cultures when compared to RI treatment at d38, 66 and 94; RA treated cultures demonstrated upregulation of HOXA3 at all points of differentiation when compared to RI treatment (** $p < 0.01$; **** $p < 0.001$). No difference was observed in FOXD3 between treatments, however, FOXD3 was significantly upregulated between d31 and days 38 and 66 ($p < 0.05$) in both RI and RA treated cultures (multiple *t*-test; n = 4 independent experiments, mean ± SD). B. Staining in RA treated cultures at d66 and d94 demonstrating development of neurite outgrowth; scale bar = 100μm. C. Merged images from scans of organoid sections from NBM alone or media supplemented with RA or RI; scale bar = 500μm. MAP2 and TUBB3 green; GFAP and O4 pink; Hoechst blue; n = 4 independent experiments. (For interpretation of the references to colour in this figure legend, the reader is referred to the web version of this article.)

3.5. Staining and analysis of replated 6 well cultured aggregates

Aggregates from all three cell lines cultured as static 6 well cultures were plated and stained for NANOG (d0), POU5F1 (d0 and d5), PAX6 (d5, d10, p1-p4), SOX1 (d10, p1-p4) and MAP2 (p1-p4). Representative images can be found in Fig. 3(WA09), Supplementary Fig. S4 (ESI-hES3) and Supplementary Fig. S5 (MEL1). Analysis of WA09 staining demonstrated significant downregulation of POU5F1 between d0 and d5 ($p < 0.001$). The percentages of PAX6 and SOX1 positive cells increased between d5 and d10 ($p < 0.005$), and p2 and p3 ($p < 0.001$), no significant difference was found at other time points. The percentage of MAP2 positive cells increased at p3 (Fig. 3A; $p < 0.001$).

No significant downregulation of POU5F1 protein expression in ESI-hES3 was found between d0 and d5, which correlated with slower down regulation on the transcript level (Supplementary Fig. S4A). However, by day 10 transcript expression of pluripotency markers were found to be statistically significantly downregulated ($p < 0.001$). Significant increases of PAX6 and SOX1 positive cells were found by immunostaining between d10 and p1 ($p < 0.001$; Supplementary Fig. S4B and C). The percentage of positive cells remained high (> 70%) until p4 when cells significantly decreased to 62% (PAX6) and 57% (SOX1; $p < 0.05$). MAP2 demonstrated an increase in the number of positive cells at p4 ($p < 0.05$), suggesting that the cells had remained at a neural stem/progenitor stage.

MEL1 exhibited downregulation of both transcript and protein levels of POU5F1 cells between d0 and d10 ($p < 0.001$) and significant upregulation of PAX6 and SOX1 between d10 and p1 to > 80% positive cells ($p < 0.001$; Supplementary Fig. S5A and B). These data demonstrate that, for all three cell lines, the majority of cells continued to express neural progenitor markers and thus the stem/progenitor cell stage was induced and maintained.

3.6. Supplementation of 3D cultures with EGF and FGF2 throughout differentiation

Previous data has reported that EGF and FGF2 can influence neural stem and progenitor cell populations (Taupin et al., 2000). To examine if extended supplementation of neural cultures with FGF2/EGF would aid in maintaining cells in at earliest neural stem cell stages we established 3D cultures to investigate effects of these factors on proliferation, aggregate diameter and gene expression. Levenstein et al. reported that during overnight incubation at 37 °C, FGF2 protein levels underwent significant decay regardless of concentration (Levenstein et al., 2006). In comparison, controlled release of FGF2 demonstrated maintenance of pluripotency in hESC (Lotz et al., 2013). The use of sustainable (thermostable) FGF2 has achieved stable maintenance of FGF2 levels within culture media thus affecting biological activity (Dvorak et al., 2018).

Following the initial 10 days of induction, 3D NBM cultures were supplemented with EGF alone, or FGF2 alone, or EGF and FGF2 added weekly, or daily, or thermostable FGF2 supplemented twice weekly (with EGF).

We compared the diameter of EGF/FGF2 supplemented aggregates using one-way ANOVA. Within individual conditions, aggregate width decreased in NBM alone from d10 onwards; p1d7 EGF alone; p2d7 FGF2 alone. EGF/FGF2, supplemented on a weekly basis, aggregates supplemented with sustainable FGF2/EGF twice weekly or on a daily basis demonstrated significant increases in width until p2d7 the decreased in width until experiment termination (p4p7; levels of significance were $p < 0.001$ for all tests; Supplementary Fig. S8A).

Analysis of aggregate diameter between different culture conditions demonstrated significant differences at most sampling points ($p < 0.001$); statistics for this analysis are in Supplementary Table S2.

Analysis of proliferation (Supplementary Fig. S8A) demonstrated no significant differences at d5 or d10 between the different culture conditions. After d10 aggregates cultured in NBM reached a plateau and no significant proliferation was observed. In comparison, supplementation with EGF or FGF2 alone demonstrated slower but sustained proliferation. EGF/FGF2 supplemented weekly, daily or the sustainable FGF2 all demonstrated increasing proliferation until p2 ($p < 0.05$).

While viability remained high at > 87% across all culture conditions NMB cultures demonstrated decreased viability across all time points when compared to EGF/FGF2 cultures ($p < 0.05$). Aggregates cultured in FGF/EGF supplemented NBM all demonstrated suppression of *PAX6*, *SOX1*, *HOXA3* and *DCX* when compared to NBM alone at p3 (Supplementary Fig. S8B, Supplementary Table S4; $p < 0.005$). *NCAM* only showed significant differences when EGF/FGF2 were supplemented together ($p < 0.005$). *MAP2* did not demonstrate any significant differences, confirming that addition of EGF/FGF2 maintained the cells as neural progenitors.

3.7. Aggregate differentiation to neurons

To establish if 3D aggregates were developmentally competent to differentiate into neurons WA09 aggregates, following dual SMAD inhibition and 5 days of neural induction with EGF and FGF2, were cultured as organoids and treated with either RA, RI or in NBM alone (Fig. 4). Studies have demonstrated that RI supplementation of murine neural stem cells increased neurite outgrowth and enhanced neuronal differentiation without affecting cell viability post replating (Jia et al., 2016). RA has demonstrated a caudalizing effect during neural induction of stem cells (Allodi and Hedlund, 2014; Liu and Zhang, 2011) and has exhibited suppression of ventral central nervous tissue (Irioka et al., 2005). Here, RA treatment, initiated following early differentiation, was associated with high levels of *HOXA3* transcript suggesting induction of a caudal neural fate. Gene expression analysis (Fig. 4A) revealed statistically significant increases in *GFAP*, *S100B*, *NEUROG1* and *EN1* in RI treated aggregates at d94 as compared to days 31, 38 and 66 or aggregates treated with RA at equivalent time points (** $p < 0.01$; *** $p < 0.005$, **** $p < 0.001$). *HOXA3* expression was significantly upregulated in RA cultures when compared with RI at equivalent time points (** $p < 0.05$ d31 RI vs d31 RA; **** $p < 0.001$ days 38, 66 and 94, RI vs RA). Staining from differentiated aggregates (Fig. 4B) supplemented for 66 days with RA demonstrated PAX6 positive rosettes as well as neurite outgrowth (MAP2 and TUBB3 staining). At day 94 only a few cells showed strong expression of PAX6; neurite outgrowth was identified using MAP2 and TUBB3.

Studies into the neurodegenerative disease aetiology have recently shown that organoid cultures provide a near-physiological in vitro model system, allowing investigation of human development, disease progression and drug discovery (Fatehullah et al., 2016; Jo et al., 2016; Lancaster et al., 2013; Mason and Price, 2016). Long-term organoid cultures have the potential to model aspects such as neuronal maturation and survival, and have been demonstrated to faithfully recapitulate early developmental aspects of the fetal brain (Kelava and Lancaster, 2016; Knowlton et al., 2016). Here, WA09 organoids, cultured for 12 weeks (NBM alone, RI treated and RA treated), were fixed and embedded in paraffin before sectioning and staining with MAP2, TUBB3, GFAP, O4, NES, and PAX6, using Alexa Fluor secondaries and Hoechst as a DNA counterstain (Fig. 4C, Supplementary Fig. S9). In addition, sections were stained with H&E and aggregate diameter was measured and compared across all three conditions. Significant differences were found in organoid diameter between NBM and the RI/RA treatments (Supplementary Fig. S9; **** $p < 0.001$). Positive staining for MAP2, TUBB3, O4, and NES were observed in NBM organoids. RI treated organoids demonstrated MAP2, TUBB3, and MAP2 staining with some areas positive for O4. In comparison with NBM and RI treated organoids, limited MAP2 and NES staining was observed in the RA condition. Neither RA nor RI treatment resulted in GFAP positive cells. PAX6 showed occasional positive cells in all three treatment conditions localised at the outer edges of the organoids.

4. Discussion

Successful clinical application of hPSC for the treatment of injury or disease in the CNS will require robust and reproducible platforms for generating the requisite numbers of cells. The nanobridge system described here is designed to generate aggregates relatively homogeneous in size and with a high formation rate, which can be readily passaged without the use of enzymatic or non-enzymatic solutions, and can undergo successful neural induction (Abbasalizadeh et al., 2012; Chen et al., 2017; Chen et al., 2014).

Within the field of neural tissue engineering, there is increasing interest in the use of 3D platforms to generate large numbers of neural progenitors for further differentiation to terminal cell types. Comparison of the efficacy of 2D vs 3D cultures of hPSC undergoing neural differentiation has been previously published with, thus far, widespread agreement that 3D cultures provide better differentiation and less apoptosis (Chandrasekaran et al., 2017; Ribeiro et al., 2010; Sadri et al., 2014). However, there has been less emphasis on the ability to serially propagate and maintain neural progenitors in these 3D systems. 3D aggregates in many current publications are routinely generated for terminal differentiation and are not subject to passaging, thus, as aggregate size increases there is the potential for necrotic cores to become established. We have validated a system where a high percentage of hESC aggregates can be formed, induced to the neural lineages and disaggregated using a thermoresponsive polymer while maintaining proliferation and viability. Staining of intact aggregates verified that live cells were evenly distributed throughout the aggregate indicating that a necrotic centre was not established possibly due to the ability to maintain control of aggregate size. However, some 94 day terminal differentiation cultures, where disaggregation was not performed, demonstrated loss of Hoechst staining in a centralised area (see Supplementary Fig. S9 RA induction). Aggregates employed for 94 day differentiation were substantially larger ($> 950\mu m$ as compared to an average diameter of 300μm) than those routinely disaggregated. Previous publications have confirmed the presence of HIF1A necrotic cores in cancer spheroids of $\approx$ 500μm and above (Daster et al., 2017; Hirschhaeuser et al., 2010).

No differences could be determined in transcript or protein expression in the presence or absence of the nanobridges, confirming that the NB did not influence the differentiation process. Across the three cell lines, six well cultures retained a high percentage viability, continued proliferation and were maintained at average aggregate diameters of between 300 and 450μm. Formation of the aggregates using the 96 well platform demonstrated high uniformity in diameter. However, static six well cultures revealed enhanced proliferation, could maintain aggregate size and progenitor status for an increased number of passages, as compared to 96 well cultures. While aggregates in the static 6 well platforms showed higher variability in diameter preliminary experiments comparing hESC cultured using spinner flasks have shown a greater uniformity in size and shape.

FGF2 has been reported to effect neural differentiation at a number of different time points. Cohen et al. showed that FGF signalling in hESC induced early neural specification (Cohen et al., 2010). Israsena et al., reported that cells cultured in the presence of FGF2 aided in maintaining the cells at the neural progenitor stage (Israsena et al., 2004) and Hu et al. described increased numbers of PAX6 cells when NBM was supplemented with FGF however their data was cell line dependant (Hu et al., 2010). Increased heterogeneity and rosette malformation has been reported during supplementation of neural stem cell cultures with FGF2 and EGF (Denham and Dottori, 2009; Elkabetz et al., 2008). During early rosette formation, FGF2 has been demonstrated to be involved in rostral-caudal patterning directing neural differentiation towards forebrain lineages (Denham and Dottori, 2009). Additionally, FGF signalling in hESC has been shown to induce, but is not essential, for early neutralization (Cohen et al., 2010). These reports suggest that FGF2 has biphasic roles during neural induction and that balancing FGF2 signalling impacts on rosette development and thus neural fate determination.

Data presented here demonstrated that, similar to Grabiec et al. where FGF2 repressed the onset of *PAX6* in differentiating hESC (Grabiec et al., 2016; Greber et al., 2011), supplementation of cultures increased proliferation but transcript levels of *PAX6* and *SOX1* were significantly decreased at p3 ($p < 0.001$ and $p < 0.05$ respectively) in all treatment conditions compared with routine NBM cultures (EGF/FGF2 withdrawn after 5 days). However, another key marker of neural differentiation, NCAM, demonstrated transcript levels comparable to those observed in NBM in EGF alone and FGF2 cultures. This dichotomy may be explained by the involvement of NCAM in cell-to-cell and cell-matrix interactions (Eggers et al., 2011).

Terminal differentiation of neural cultures provides an important proof-of-concept for the aggregates' developmental capacity. We have demonstrated that growth in the presence of NB does not inhibit differentiation to neurons and that when plated the neurons can outgrow and are positive for TUBB3 and MAP2. Additionally, organoid cultures treated with RI differentiated towards a neuronal phenotype. In contrast, RA treated cultures differentiated to a limited amount of oligodendrocyte and astrocyte cells suggesting that cultures did not differentiate into glial cells. Interestingly, cells grown in NBM alone contained cells expressing markers of both oligodendrocyte and glial cells as well as neurones, as evidenced by staining. The 3D cultures using the NB can provide a robust method for terminal differentiation. Further investigations are needed to provide functionality of the terminally differentiated cells and to determine, using in vivo models, if cells formed in aggregates using NB are competent to integrate into CNS tissue, vascularise and repair injury.

In conclusion, we have established the capability of the nanobridge system to generate hESC aggregates that can undergo neuronal differentiation and be expanded and maintained at a stem/progenitor stage. In addition, aggregates have the capacity to differentiate towards a more mature phenotype as demonstrated by outgrowth of neurites. The nanobridge system has no impact on the differentiation process, proliferation or cell viability but aids in maintaining dissociation and re-aggregation of the cells. The use of a two-component polymer conjugated to a small fragment of fibronectin offers the prospect of adaptability of this system. Small fragments of alternative ECMs, such as Laminin or Vitronectin, or combinations of ECMs could be utilised for either alternative lineages or to specify cell type. Our study suggests that the 3D aggregate cultures are a significantly more effective culture system in the early stages of differentiation. The 6 well culture platform is an initial step towards scale-up bioreactor systems which could generate bulk cultures of hPSC undergoing neural differentiation. This would allow either for the sampling and distribution of cultures for use atprogenitor stages or for more terminally differentiated cell types. Moreover, our system provides a platform for uniform and consistent generation of large-scale culture of CNS organoid progenitors, which has several advantages over existing systems for producing organoids. Our research provides a step towards developing a sustainable and cost effective platform for furthering the use of stem cells in clinical applications and drug discovery.

Supplementary data to this article can be found online at https://doi.org/10.1016/j.scr.2019.101441.

Ethical approval

Ethical approval for experimental use of hESC lines was given by The University of Queensland Medical Research Ethics Committee.

Author contributions

LH and XC performed the cell cultures, live imaging and analysis; LH performed the staining, qPCR and resultant analysis; LH and AMD performed the InCell imaging and analysis; ZJ and MM developed and

manufactured the NB; XC functionalised the NB; PG and MP developed the study concept, supervised the research team, and contributed to experimental design and planning. All authors were involved in the manuscript preparation and editing.

Acknowledgements

The authors would like to acknowledge funding from Stem Cells Australia, an Australian Research Council Strategic Initiative in Stem Cell Science (SR110001002), the JEM Research Foundation philanthropic funding, The Merchant Charitable Foundation and the University of Queensland for their support and funding of this work. This work was performed in part at the Queensland node of the Australian National Fabrication Facility. A company established under the National Collaborative Research Infrastructure Strategy to provide nano and microfabrication facilities for Australia's researchers. The authors declare no conflict of interest.

References

Abbasalizadeh, S., Larijani, M.R., Samadian, A., Baharvand, H., 2012. Bioprocess development for mass production of size-controlled human pluripotent stem cell aggregates in stirred suspension bioreactor. Tissue Eng. C Methods 18, 831–851.
Adil, M.M., Rodrigues, G.M., Kulkarni, R.U., Rao, A.T., Chernavsky, N.E., Miller, E.V., Schaffer, D.V., 2017. Efficient generation of hPSC-derived midbrain dopaminergic neurons in a fully defined, scalable, 3D biomaterial platform. Sci. Rep. 7, 40573 Jan 16.
Akkerman, N., Defize, L.H., 2017. Dawn of the Organoid Era: 3D Tissue and Organ Cultures Revolutionize the Study of Development, Disease, and Regeneration. BioEssays : News and Reviews in Molecular, Cellular and Developmental Biology *39*.
Allodi, I., Hedlund, E., 2014. Directed midbrain and spinal cord neurogenesis from pluripotent stem cells to model development and disease in a dish. Front. Neurosci. 8, 109.
Bozza, A., Coates, E.E., Incitti, T., Ferlin, K.M., Messina, A., Menna, E., Bozzi, Y., Fisher, J.P., Casarosa, S., 2014. Neural differentiation of pluripotent cells in 3D alginate-based cultures. Biomaterials 35, 4636–4645.
Chambers, S.M., Fasano, C.A., Papapetrou, E.P., Tomishima, M., Sadelain, M., Studer, L., 2009. Highly efficient neural conversion of human ES and iPS cells by dual inhibition of SMAD signaling. Nat. Biotechnol. 27, 275–280.
Chambers, S.M., Qi, Y., Mica, Y., Lee, G., Zhang, X.J., Niu, L., Bilsland, J., Cao, L., Stevens, E., Whiting, P., et al., 2012. Combined small-molecule inhibition accelerates developmental timing and converts human pluripotent stem cells into nociceptors. Nat. Biotechnol. 30, 715–720.
Chandrasekaran, A., Avci, H.X., Ochalek, A., Rosingh, L.N., Molnar, K., Laszlo, L., Bellak, T., Teglasi, A., Pesti, K., Mike, A., et al., 2017. Comparison of 2D and 3D neural induction methods for the generation of neural progenitor cells from human induced pluripotent stem cells. Stem Cell Res. 25, 139–151.
Chen, X., Pan, W., 2014. The treatment strategies for neurodegenerative diseases by integrative medicine. Integr. Med. Int. 1, 223–225.
Chen, V.C., Couture, S.M., Ye, J., Lin, Z., Hua, G., Huang, H.I., Wu, J., Hsu, D., Carpenter, M.K., Couture, L.A., 2012. Scalable GMP compliant suspension culture system for human ES cells. Stem Cell Res. 8, 388–402.
Chen, X., Prowse, A.B., Jia, Z., Tellier, H., Munro, T.P., Gray, P.P., Monteiro, M.J., 2014. Thermoresponsive worms for expansion and release of human embryonic stem cells. Biomacromolecules 15, 844–855.
Chen, X., Harkness, L., Jia, Z., Prowse, A., Monteiro, M., Gray, P.P., 2018. Methods for expansion of 3D cultures of human embryonic stem cells using a Thermoresponsive polymer. Tissue Eng. C Methods 24 (3), 146–157.
Cohen, M.A., Itsykson, P., Reubinoff, B.E., 2010. The role of FGF-signaling in early neural specification of human embryonic stem cells. Dev. Biol. 340, 450–458.
Daster, S., Amatruda, N., Calabrese, D., Ivanek, R., Turrini, E., Droeser, R.A., Zajac, P., Fimognari, C., Spagnoli, G.C., Iezzi, G., et al., 2017. Induction of hypoxia and necrosis in multicellular tumor spheroids is associated with resistance to chemotherapy treatment. Oncotarget 8, 1725–1736.
Dehmelt, L., Halpain, S., 2005. The MAP2/tau family of microtubule-associated proteins. Genome Biol. 6, 204.
Denham, M., Dottori, M., 2009. Signals involved in neural differentiation of human embryonic stem cells. Neurosignals 17, 234–241.
Dvorak, P., Bednar, D., Vanacek, P., Balek, L., Eiselleova, L., Stepankova, V., Sebestova, E., Kunova Bosakova, M., Konecna, Z., Mazurenko, S., et al., 2018. Computer-assisted engineering of hyperstable fibroblast growth factor 2. Biotechnol. Bioeng. 115, 850–862.
Edmondson, R., Broglie, J.J., Adcock, A.F., Yang, L., 2014. Three-dimensional cell culture systems and their applications in drug discovery and cell-based biosensors. Assay Drug Dev. Technol. 12, 207–218.
Eggers, K., Werneburg, S., Schertzinger, A., Abeln, M., Schiff, M., Scharenberg, M.A., Burkhardt, H., Muhlenhoff, M., Hildebrandt, H., 2011. Polysialic acid controls NCAM signals at cell-cell contacts to regulate focal adhesion independent from FGF receptor activity. J. Cell Sci. 124, 3279–3291.
Elkabetz, Y., Panagiotakos, G., Al Shamy, G., Socci, N.D., Tabar, V., Studer, L., 2008. Human ES cell-derived neural rosettes reveal a functionally distinct early neural stem cell stage. Genes Dev. 22, 152–165.
Fatehullah, A., Tan, S.H., Barker, N., 2016. Organoids as an in vitro model of human development and disease. Nat. Cell Biol. 18, 246–254.
Filipovic, R., Santhosh Kumar, S., Fiondella, C., Loturco, J., 2012. Increasing doublecortin expression promotes migration of human embryonic stem cell-derived neurons. Stem Cells 30, 1852–1862.
Grabiec, M., Hribkova, H., Varecha, M., Stritecka, D., Hampl, A., Dvorak, P., Sun, Y.M., 2016. Stage-specific roles of FGF2 signaling in human neural development. Stem Cell Res. 17, 330–341.
Greber, B., Coulon, P., Zhang, M., Moritz, S., Frank, S., Muller-Molina, A.J., Arauzo-Bravo, M.J., Han, D.W., Pape, H.C., Scholer, H.R., 2011. FGF signalling inhibits neural induction in human embryonic stem cells. EMBO J. 30, 4874–4884.
Hama, H., Kurokawa, H., Kawano, H., Ando, R., Shimogori, T., Noda, H., Fukami, K., Sakaue-Sawano, A., Miyawaki, A., 2011. Scale: a chemical approach for fluorescence imaging and reconstruction of transparent mouse brain. Nat. Neurosci. 14, 1481–1488.
Hirschhaeuser, F., Menne, H., Dittfeld, C., West, J., Mueller-Klieser, W., Kunz-Schughart, L.A., 2010. Multicellular tumor spheroids: an underestimated tool is catching up again. J. Biotechnol. 148, 3–15.
Hu, B.Y., Weick, J.P., Yu, J., Ma, L.X., Zhang, X.Q., Thomson, J.A., Zhang, S.C., 2010. Neural differentiation of human induced pluripotent stem cells follows developmental principles but with variable potency. PNAS 107, 4335–4340.
Huch, M., Knoblich, J.A., Lutolf, M.P., Martinez-Arias, A., 2017. The hope and the hype of organoid research. Development 144, 938–941.
Irioka, T., Watanabe, K., Mizusawa, H., Mizuseki, K., Sasai, Y., 2005. Distinct effects of caudalizing factors on regional specification of embryonic stem cell-derived neural precursors. Brain Res. Dev. Brain Res. 154, 63–70.
Israsena, N., Hu, M., Fu, W., Kan, L., Kessler, J.A., 2004. The presence of FGF2 signaling determines whether beta-catenin exerts effects on proliferation or neuronal differentiation of neural stem cells. Dev. Biol. 268, 220–231.
Jia, X.F., Ye, F., Wang, Y.B., Feng, D.X., 2016. ROCK inhibition enhances neurite outgrowth in neural stem cells by upregulating YAP expression in vitro. Neural Regen. Res. 11, 983–987.
Jo, J., Xiao, Y., Sun, A.X., Cukuroglu, E., Tran, H.D., Goke, J., Tan, Z.Y., Saw, T.Y., Tan, C.P., Lokman, H., et al., 2016. Midbrain-like Organoids from human pluripotent stem cells contain functional dopaminergic and Neuromelanin-producing neurons. Cell Stem Cell 19, 248–257.
Kelava, I., Lancaster, M.A., 2016. Dishing out mini-brains: current progress and future prospects in brain organoid research. Dev. Biol. 420, 199–209.
Knowlton, S., Cho, Y., Li, X.J., Khademhosseini, A., Tasoglu, S., 2016. Utilizing stem cells for three-dimensional neural tissue engineering. Biomater. Sci. 4, 768–784.
Lancaster, M.A., Renner, M., Martin, C.-A., Wenzel, D., Bicknell, L.S., Hurles, M.E., Homfray, T., Penninger, J.M., Jackson, A.P., Knoblich, J.A., 2013. Cerebral organoids model human brain development and microcephaly. Nature 501, 373–379.
Levenstein, M.E., Ludwig, T.E., Xu, R.H., Llanas, R.A., VanDenHeuvel-Kramer, K., Manning, D., Thomson, J.A., 2006. Basic fibroblast growth factor support of human embryonic stem cell self-renewal. Stem Cells 24, 568–574.
Li, H., Wijekoon, A., Leipzig, N.D., 2012. 3D differentiation of neural stem cells in macroporous photopolymerizable hydrogel scaffolds. PLoS ONE 7, e48824.
Liu, H., Zhang, S.C., 2011. Specification of neuronal and glial subtypes from human pluripotent stem cells. Cell. Mol. Life Sci. 68, 3995–4008.
Lotz, S., Goderie, S., Tokas, N., Hirsch, S.E., Ahmad, F., Corneo, B., Le, S., Banerjee, A., Kane, R.S., Stern, J.H., et al., 2013. Sustained levels of FGF2 maintain undifferentiated stem cell cultures with biweekly feeding. PLoS ONE 8, e56289.
Mansour, A.A., Goncalves, J.T., Bloyd, C.W., Li, H., Fernandes, S., Quang, D., Johnston, S., Parylak, S.L., Jin, X., Gage, F.H., 2018. An in vivo model of functional and vascularized human brain organoids. Nat. Biotechnol. 36 (5), 432–441.
Martin, P., Wimo, A., Guerchet, M., Ali, G.-C., Wu, Y.-T., Prina, M., 2015. The Global Impact of Dementia: an Analysis of Prevalence, Incidence, Cost and Trends (London). (pp. 87).
Mason, J.O., Price, D.J., 2016. Building brains in a dish: prospects for growing cerebral organoids from stem cells. Neuroscience 334, 105–118.
Philippidou, P., Dasen, J.S., 2013. Hox genes: choreographers in neural development, architects of circuit organization. Neuron 80, 12–34.
Ribeiro, A.P., Powell, E.M., Leach, J.B., 2010. Neural Stem Cell Differentiation in 2D and 3D Microenvironments. Paper Presented at: IFMBE Proceedings (Springerlink).
Rodrigues, G.M.C., Gaj, T., Adil, M.M., Wahba, J., Rao, A.T., Lorbeer, F.K., Kulkarni, R.U., Diogo, M.M., Cabral, J.M.S., Miller, E.W., Hockemeyer, D., Schaffer, D.V., 2017. Defined and scalable differentiation of human oligodendrocyte precursors from pluripotent stem cells in a 3d culture system. Stem Cell Rep. 8 (6), 1770–1783 2017.
Sadri, S., Khazaei, M., Ghanbari, A., Khazaei, M.R., Shah, P., 2014. Neuronal differentiation of PC12 and embryonic stem cells in two- and three-dimensional in vitro culture. Indian J. Exp. Biol. 52, 305–311.
Schneider, C.A., Rasband, W.S., Eliceiri, K.W., 2012. NIH Image to ImageJ: 25 years of image analysis. Nat. Methods 9, 671–675.
Taupin, P., Ray, J., Fischer, W.H., Suhr, S.T., Hakansson, K., Grubb, A., Gage, F.H., 2000. FGF-2-responsive neural stem cell proliferation requires CCg, a novel autocrine/paracrine cofactor. Neuron 28, 385–397.
Wang, X., Dai, J., 2010. Concise review: isoforms of OCT4 contribute to the confusing diversity in stem cell biology. Stem Cells 28, 885–893.
Wattanapanitch, M., Klincumhom, N., Potirat, P., Amornpisutt, R., Lorthongpanich, C., Upratya, Y., Laowtammathron, C., Kheolamai, P., Poungvarin, N., Issaragrisil, S., 2014. Dual small-molecule targeting of SMAD signaling stimulates human induced pluripotent stem cells toward neural lineages. PLoS ONE 9, e106952.
Werner, S., Vu, H.T., Rink, J.C., 2016. Self-organization in development, regeneration and organoids. Curr. Opin. Cell Biol. 44, 102–109.